

Imprinting Ground State Chirality on Adatom Spins

Yun-Peng Huang^{1,*} and Panagiotis Kotetes^{2,†}

¹*Beijing National Laboratory for Condensed Matter Physics, and Institute of Physics, Chinese Academy of Sciences, Beijing 100190, China*

²*CAS Key Laboratory of Theoretical Physics, Institute of Theoretical Physics, Chinese Academy of Sciences, Beijing 100190, China*

We propose an alternative experimental protocol for the detection of doped Chern insulators and chiral superconductors. Our approach relies on coupling the target chiral system to adatom spins. Due to the substrate chirality, the adatom spins are expected to order in a noncoplanar configuration with a nonzero spin chirality. Here, we obtain concrete results for chiral substrates which are invariant under arbitrary spin rotations, and are coupled to three adatoms carrying classical moments. By exploring all the accessible magnetic ground states, we identify the regimes in which nonzero spin chirality is induced on the adatom complex. We apply our method to valley-polarized bilayer graphene and $d + id$ superconductors, and find qualitatively different ground state diagrams. Our analysis shows that the adatom spin chirality fully encodes the properties of the substrate chirality.

Introduction – While the unambiguous identification of two-dimensional topological systems which simultaneously violate parity and time-reversal symmetries [1–3] is highly desirable, it yet remains a formidable task. There exist two main experimental strategies which in principle allow us to detect these also-called chiral systems, i.e., either to observe their topologically protected chiral edge modes, or, to diagnose the nonzero chirality arising in the bulk. In the former approach, one is typically required to carry out quantum transport experiments [4–6], which apart from being extremely challenging to conduct, they may also be inconclusive due to the strong dependence of the measured quantities on the boundary conditions and the possible presence of disorder [7]. On the other hand, the detection of the ground state chirality usually relies on circular-polarization-sensitive responses [8, 9], such as the polar Kerr effect (PKE) [10]. In spite of the high resolution which is found in state-of-the-art PKE experiments [11], the precise microscopic origin of the observed PKE signal is not always identifiable. A well-known example here is Sr_2RuO_4 , for which a PKE was observed early on [12], but the type of the pairing gap which breaks time reversal-symmetry still remains unsettled [13].

In this Letter, we bring forward an alternative method to detect the ground state chirality. We propose to couple the target chiral system to adatom spins, and monitor the type of ground state which gets stabilized due to the coupling of the spins to the substrate. The minimal configuration which can encode a nonzero ground state chirality is three spins, and is schematically depicted in Fig. 1. Here, the adatoms are modeled as point-like objects whose magnetic moments are treated as classical spins. The key observation underlying our detection proposal is that, when the substrate is chiral, the ground state of the spins is expected to possess a nonzero spin chirality χ_C [14–16]. The latter is a measure of the degree of the noncoplanarity of the adatom spin configuration. Hence, the detection of spin chirality promises to provide an indirect signature of the substrate chirality.

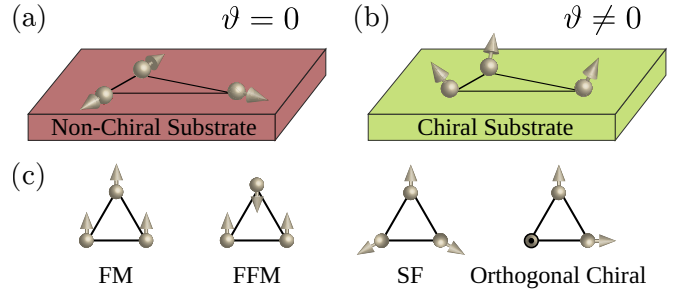


FIG. 1. Minimal three-adatom setup for the detection of substrate chirality. For a substrate with spin rotational invariance, the adatom spins order in a coplanar fashion when the chirality is zero, as depicted in (a). In contrast, a nonzero chirality promotes a noncoplanar chiral magnetic pattern, see (b). (c) shows the possible magnetic ground states. A non-chiral substrate allows for ferromagnetic (FM), frustrated ferromagnetic (FFM), and spin flux (SF) ground states. When the chirality is switched on, the SF state adiabatically evolves into a noncoplanar chiral state. When chiral spin interactions dominate, the spins order in an orthogonal chiral fashion.

We draw concrete conclusions for chiral substrates which are invariant under arbitrary spin rotations. By integrating out the substrate electrons, we obtain an effective functional for the adatom spins which consists of the usual Ruderman-Kittel-Kasuya-Yosida (RKKY) two-spin interaction [17], along with a chiral three-spin interaction [2, 16] which encodes the substrate chirality. By identifying all the possible ground states of the spins, we conclude that, when the usual RKKY term favors ferromagnetic ordering, a nonzero spin chirality can be induced on the spins discontinuously, and only after the strength of the chiral spin interaction reaches a certain threshold. In contrast, when the RKKY term favors anti-ferromagnetism, a nonzero spin chirality can be induced continuously on the adatom spins. We make predictions for valley polarized bilayer graphene and $d + id$ superconductors. We find that these systems exhibit qualitatively different Friedel oscillations and spin chiralities.

Representative Model Hamiltonian – We consider the single-particle two-band Hamiltonian $\hat{H}(\mathbf{k}) = \mathbf{d}(\mathbf{k}) \cdot \boldsymbol{\tau} - d_0 \hat{1}_\tau$, which depends on the wave vector $\mathbf{k} = (k_x, k_y)$, and is identical for both spins. In the above, $\tau_{1,2,3}$ define Pauli matrices and $\hat{1}_\tau$ the respective identity matrix. From now on, we omit writing the identity matrix to simplify the notation. Here, d_0 defines a generalized chemical potential while we choose $\mathbf{d}(\mathbf{k})$ as:

$$\mathbf{d}(\mathbf{k}) = \frac{\Delta}{k_0^2} \left(k_x^2 - k_y^2, 2k_x k_y, V(\mathbf{k}^2 - k_0^2)/\Delta \right). \quad (1)$$

Depending on the case, the two-state τ basis can relate to orbital, sublattice, Nambu, or other degrees of freedom.

Effective Spin Interactions – We assume that the substrate electrons couple to a number of N adatom spins \mathbf{S}_i which are deposited at positions \mathbf{R}_i , by means of the exchange interactions $H_J = J \sum_{i=1}^N \mathbf{S}_i \cdot \hat{\mathbf{s}}_i$. Here, J controls the strength of the coupling and $\hat{\mathbf{s}}_i$ is the electronic spin operator. In the remainder we set $|\mathbf{S}_i| = 1$. By integrating out the substrate electrons, we derive an effective energy functional E_{spins} which contains the multi-spin interactions. For this purpose, we assume that the exchange coupling is sufficiently small, so that we can neglect possible bound states induced by the adatoms [18]. Under this condition, we treat the substrate-adatom coupling perturbatively, and consider only the contribution of the itinerant electrons [19–21]. Since in this work it is crucial to capture the nonzero chirality dictating the substrate, it is important to expand at least up to third order in the coupling J . By doing so, we find that E_{spins} is a sum of two parts. The first is the usual RKKY term:

$$E_{\text{RKKY}} = -\frac{J^2}{2} \sum_{i,j} \chi_{ij} \mathbf{S}_i \cdot \mathbf{S}_j \quad (2)$$

while the second encodes the three-spin chiral coupling:

$$E_{\text{Chiral}} = -\frac{J^3}{6} \sum_{i,j,k} \vartheta_{ijk} \mathbf{S}_i \cdot (\mathbf{S}_j \times \mathbf{S}_k). \quad (3)$$

The chiral spin interaction has so far been discussed in various contexts. It first appeared in the field of spin liquids [14–16], which remains up to now an open research topic [22–25]. While in these studies the chiral spin interaction is treated phenomenologically, other works have discussed how this emerges in the presence of a magnetic field [26, 27]. More recently, it was emphasized that chiral spin terms can also be engineered in topological systems whose bands carry a nonzero Berry curvature [28–30], without any requirement for an external magnetic field.

Our goal is to evaluate the two- and three-spin susceptibilities $\chi_{ij} \equiv \chi(\mathbf{R}_i, \mathbf{R}_j)$ and $\vartheta_{ijk} \equiv \vartheta(\mathbf{R}_i, \mathbf{R}_j, \mathbf{R}_k)$. In the zero temperature limit, these are defined as:

$$\chi_{ij} = -2 \int \frac{d\varepsilon}{2\pi} \text{tr} \left[\hat{G}(\varepsilon, \mathbf{R}_{ij}) \hat{G}(\varepsilon, \mathbf{R}_{ji}) \right], \quad (4)$$

$$\vartheta_{ijk} = -4t \int \frac{d\varepsilon}{2\pi} \text{tr} \left[\hat{G}(\varepsilon, \mathbf{R}_{ij}) \hat{G}(\varepsilon, \mathbf{R}_{jk}) \hat{G}(\varepsilon, \mathbf{R}_{ki}) \right], \quad (5)$$

where tr denotes trace in τ space and $\mathbf{R}_{ij} = \mathbf{R}_i - \mathbf{R}_j$. When τ labels electron and hole states of a superconductor, a factor of $1/2$ needs to be added to Eqs. (4) and (5) to avoid double counting the electronic degrees of freedom.

We observe that the coefficients χ_{ij} and ϑ_{ijk} depend only on the differences of the adatom positions, since the substrate is assumed to be invariant under arbitrary spatial translations. The two susceptibilities are expressed in terms of the coordinate space matrix Green function:

$$\hat{G}(\varepsilon, \mathbf{R}) = \int \frac{d\mathbf{k}}{(2\pi)^2} e^{i\mathbf{k} \cdot \mathbf{R}} \hat{G}(\varepsilon, \mathbf{k}), \quad (6)$$

which is the Fourier transform of the Euclidean matrix Green function $\hat{G}(\varepsilon, \mathbf{k}) = 1/[\imath\varepsilon - \hat{H}(\mathbf{k})]$, where $\varepsilon \in (-\infty, +\infty)$ defines the imaginary energy. We provide technical details in our supplemental material [31].

Magnetic Ground States of Three Adatoms – In order to experimentally detect the nonzero chirality of the substrate, it is crucial to first identify the set of ground states that become accessible for the minimal setup which consists of three adatoms at positions $\mathbf{R}_{1,2,3}$ carrying magnetic moments $\mathbf{S}_{1,2,3}$, respectively. By combining the RKKY and chiral contributions of Eqs. (2) and (3), the corresponding spin functional takes the form:

$$E_{\text{spins}} = -J^2 (\chi_{12} \mathbf{S}_1 \cdot \mathbf{S}_2 + \chi_{13} \mathbf{S}_1 \cdot \mathbf{S}_3 + \chi_{23} \mathbf{S}_2 \cdot \mathbf{S}_3) - J^3 \vartheta \mathbf{S}_1 \cdot (\mathbf{S}_2 \times \mathbf{S}_3), \quad (7)$$

where we set $\vartheta = \vartheta_{123}$. Given the coupling coefficients $\chi_{12}, \chi_{13}, \chi_{23}$ and ϑ , we extremize E_{spins} and infer all the possible magnetic ground states. For details see Ref. 31.

By first setting $\vartheta = 0$ and allowing for general positions $\mathbf{R}_{1,2,3}$, we find three types of magnetic extrema: (i) a ferromagnetic (FM) state with all spins aligned, (ii) the here-termed frustrated ferromagnetic (FFM) state where one spin is flipped compared to the FM state, and (iii) the coplanar spin flux (SF) state, where the spins are all pointing mostly inwards or mostly outwards, thus giving rise to a “combed” planar spin “hedgehog”. When the adatoms form an equilateral triangle, the spins in the SF state for an ideal “hedgehog” pattern with the spin flux flowing inwards or outwards being maximal, since successive spins form an angle of $2\pi/3$, as depicted in Fig. 1(c). Straightforward manipulations show that in the equilateral triangle setup, where $\chi_{12,13,23} \equiv \chi$, the FM state is the ground state for $\chi > 0$ with an energy $E_{\text{FM}} = -3J^2|\chi|$, while SF becomes stabilized for $\chi < 0$ with an energy $E_{\text{SF}} = -3J^2|\chi|/2$. As a result, the FFM does not appear in this highly symmetric adatom setup.

When ϑ is switched on, one finds three ground states once again, i.e., the FM and FFM states discussed above, along with a chiral magnetic (CM) state which possesses a nonzero spin chirality $\chi_C = \mathbf{S}_1 \cdot (\mathbf{S}_2 \times \mathbf{S}_3)$ [16]. The CM ground state enjoys maximum spin chirality when the spins are orthogonal to each other, as shown in Fig. 1(c). This here-termed orthogonal CM state, is achievable in

an equilateral triangle setup when the magnitude of the RKKY susceptibility $|\chi|$ is much smaller than $|J\vartheta|$. A sweet spot where this inequality is automatically satisfied is when χ vanishes while at the same time ϑ is nonzero.

We now investigate the competition of the CM state and the collinear ones for the two possible signs of χ . For $\chi > 0$ the CM competes with FM. We find that the CM ground state is accessible only for $|J\vartheta| \geq \sqrt{3}\chi$. Remarkably, in the same interval that the CM state is well-defined, it also becomes the ground state, with its energy being exactly equal to $E_{\text{FM}} = -3J^2\chi$ at $|J\vartheta| = \sqrt{3}\chi$, and further decreasing for $|J\vartheta|/\chi > \sqrt{3}$. Hence, for $\chi > 0$, a threshold value $|J\vartheta|/\chi = \sqrt{3}$ is required to be reached so to induce spin chirality on the adatoms.

In stark contrast, when $\chi = -|\chi| < 0$, the CM solution is always accessible. As a matter of fact, in this parameter regime, the limit $\vartheta \rightarrow 0$ is well-defined and the CM state energy becomes equal to $-3J^2|\chi|/2$. Hence, the CM state evolves into the SF state, thus, implying that SF and CM states are adiabatically connected and constitute the ground states of the adatom complex for $\chi < 0$. Also here, the FFM state does not get stabilized.

It is important here to point out that the chiral spin interaction acts as a ‘‘catalyst’’ for noncoplanar phases carrying a nonzero spin chirality. We find that when the ground state is nonchiral and the FM state is stabilized, switching on ϑ does not immediately induce a nonzero spin chirality on the adatoms. However, when starting from the SF state, chirality is immediately sourced by a nonzero ϑ . An analogous phenomenon was previously discussed for bulk two-dimensional itinerant magnets in prior works of ours [29, 30]. There, we showed that switching on a chiral interaction on top of the so-called spin-vortex [32, 33] or spin-whirl crystal phases [33] induces adiabatically two distinct types of spin-skyrmion crystal phases. The adiabatic evolution of nonskyrmion phases into skyrmionic ones is possible, because the spin-vortex and -whirl textures carry topological charges [33].

A similar situation takes place here for the system of the three adatoms. For $\vartheta = 0$, the SF state is the only one which carries a nontrivial topological charge, which gives rise to a nonzero vector spin chirality [34, 35]. This is precisely the reason why the SF ground state enables the induction of scalar spin chirality even upon adding an infinitesimally weak chiral interaction. However, this is not possible when starting from the FM state due its topological incompatibility with the CM state. Therefore, here, spin chirality can be only induced discontinuously.

Valley-Polarized Bilayer Graphene – A prominent realization of Chern insulators [3, 29, 36–43], can be found in bilayer graphene. In the low-energy regime, bilayer graphene can be effectively modeled by means of a two band Hamiltonian per valley [44]. Each valley Hamiltonian takes the general form shown in Eq. (1). In the present case, the τ basis is spanned by electrons living on sublattice A of one layer and electrons of sub-

lattice B of the other layer. Note that A and B correspond to the two sublattices comprising the honeycomb lattice. The mapping of Eq. (1) to the model of Ref. 44 is achieved by setting $\Delta = \gamma_1/2$ and $k_0 = \gamma_1/\sqrt{2}\hbar v_g$. Here, $\gamma_1 \simeq 390$ meV is the energy scale of the dominant interlayer coupling, $v_g \simeq 8 \cdot 10^5$ m/s is the Dirac velocity of graphene, and \hbar defines the reduced Planck constant. Our analysis neglects the effects of trigonal warping, since here we restrict to the relatively high-energy regime. In this limit, the Fermi surface consists of a single big pocket [44]. The spin-chirality phenomena predicted in this work become accessible only when a net valley polarization is present [45]. For instance, this can take place when the parameter V differs for the two valleys. The variable V corresponds to the half-difference of the electrochemical potentials defined for the two layers and is typically engineered by gating the bilayer [46–48].

By means of straightforward analytical calculations and a few standard approximations [31], we recover the known expression for the susceptibility of a given valley:

$$\chi_{\text{valley}} = \frac{4\nu_F k_F^2}{\pi} \frac{\sin(2k_F R)}{(2k_F R)^2}, \quad (8)$$

which was previously found in Ref. 49. Notably, this result is substantially modified away from the low-energy limit [50–53]. In the above, we defined the interatom distance $R > 0$, the Fermi wavenumber k_F , and the density of states ν_F at the Fermi level which is set by the chemical potential $d_0 = E_F$. From Ref. 44 we find that:

$$\frac{k_F}{k_0} = \sqrt{\frac{V^2 + \sqrt{(\Delta^2 + V^2)E_F^2 - (V\Delta)^2}}{V^2 + \Delta^2}}, \quad (9)$$

$$\nu_F = \frac{k_0^2}{4\pi} \frac{E_F}{\sqrt{(\Delta^2 + V^2)E_F^2 - (V\Delta)^2}}. \quad (10)$$

In the same spirit, we now obtain the chiral susceptibility for the case of an equilateral triangle with an adatom distance which is denoted R . For a single valley we have:

$$\vartheta_{\text{valley}} = \frac{3!(\nu_F k_F)^2}{\sqrt{8\pi/3}} \left(1 - \frac{k_0^2}{k_F^2}\right) \frac{k_F^6}{k_0^6} \frac{V\Delta^2}{E_F^3} \frac{\sin(3k_F R - \frac{3\pi}{4})}{(k_F R)^{5/2}}. \quad (11)$$

We remark that the result for a general triangular configuration is presented in Ref. 31. From the above, we observe that the chiral susceptibility is odd under $V \mapsto -V$. Based on this property we indeed confirm that for time-reversal-symmetric bilayer graphene the two valleys carry opposite chirality which cancels the total ϑ . Hence, the outcome for the induced adatom chirality strongly depends on the degree of valley polarization which is maximized when the two valleys feel identical gaps V .

In Fig. 2, we show representative results for an equilateral triangular spin setup, when accounting for both \mathbf{K} and \mathbf{K}' valleys. We define the valley polarization

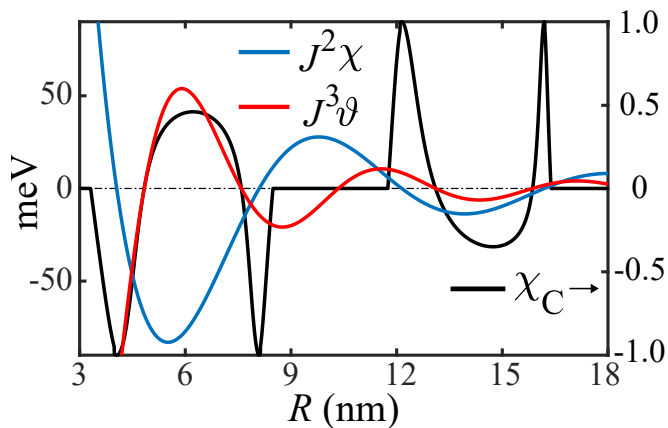


FIG. 2. RKKY and chiral coefficients χ and ϑ as a function of the interadatom distance R , for an equilateral triangle of three adatom spins coupled to bilayer graphene. By choosing $V_{\mathbf{K}} = 90$ meV and $V_{\mathbf{K}'} = -10$ meV, we obtain a valley polarization degree $VP = 0.8$. We further set $E_F = 110$ meV and $Jk_F^2 = 0.9$ eV. The spin chirality χ_C is nonzero only in the CM state, it becomes maximized when $\chi = 0$, while its sign tracks the sign of ϑ . For $\vartheta = 0$ and $\chi > 0$ ($\chi < 0$) the spins order in the FM (SF) configuration with $\chi_C = 0$.

degree as $VP = |V_{\mathbf{K}} + V_{\mathbf{K}'}| / (|V_{\mathbf{K}}| + |V_{\mathbf{K}'}|)$ and show results for $VP = 0.8$. We observe that the ground state mainly alternates between the FM and CM states, while the SF state is stabilized when $\vartheta = 0$ and $\chi < 0$. The spin chirality is nonzero in the CM state with maxima appearing for $\chi = 0$. Notably, these maxima are easily reachable since the two susceptibilities are dictated by a different sinusoidal dependence on R . When instead $|\chi| \sim |J\vartheta|$, we find moderate values for the spin chirality.

Application to chiral superconductors – Our model in Eq. (1) also applies to $d + id$ spin-singlet superconductors [1, 3, 54] after setting $d_0 = 0$. In contrast to the case of bilayer graphene, here the Fermi level is set by $V = E_F$. The two-level τ Hilbert space is spanned by electron and hole states, which describe Cooper pairs with a gap $\Delta > 0$. Also here we follow the same approach [31]. Specifically, we employ the quasi-classical approximation $E_F \gg \Delta$ and further restrict to situations where the largest interadatom distance is much smaller than the superconducting coherence length $\xi_{sc} = \hbar v_F / \Delta$, where v_F is the Fermi velocity in the normal phase. Our calculations [31] recover the known result [55]:

$$\chi_{d+id} = \frac{4\nu_F k_F^2}{\pi} \left[\frac{\sin(2k_F R)}{(2k_F R)^2} - \frac{\pi}{4} \frac{1}{k_F^2 \xi_{sc} R} \right], \quad (12)$$

where in the present case k_F coincides with k_0 , and the normal phase density of states at the Fermi level is defined as $\nu_F = k_F / 2\pi\xi\Delta$. The first term corresponds to the familiar RKKY interaction obtained when the substrate is a good metal. On the other hand, the second term appears only in the presence of the spin-singlet pair-

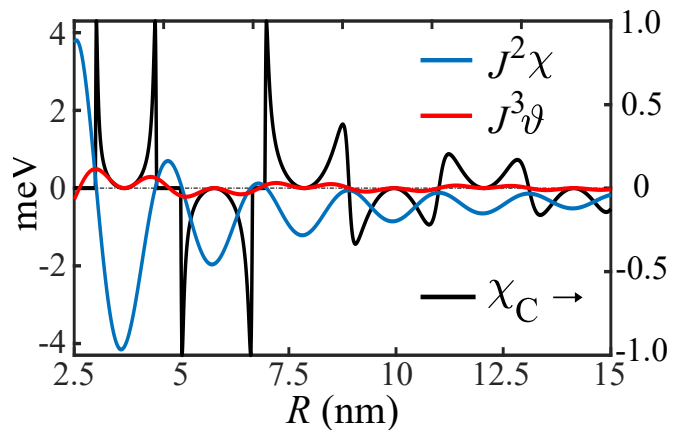


FIG. 3. Same as in Fig. 2, but for spins coupled to a $d + id$ superconductor. Here, we set $\Delta = 8$ meV, $\xi_{sc} = 50$ nm, $E_F = 300$ meV, and $Jk_F^2 = 1$ eV. The presence of the spin-singlet pairing gap strongly affects the sign and Friedel oscillation period of the two coefficients, thus promoting the CM state.

ring gap [55]. As it has been previously pointed out [56–58], this second term can dominate the RKKY susceptibility and favors antiferromagnetic ordering. This behavior stems from the spin-singlet character of the pairing and tends to promote the CM over the FM ground state.

Under the same approximations, we derive the coefficient of the chiral spin interaction, which reads as:

$$\vartheta_{d+id} = -(6\pi)^{\frac{3}{2}} \nu_F^3 \Delta \frac{\cos^2(k_F R - \frac{\pi}{4}) \sin(k_F R - \frac{\pi}{4})}{(k_F R)^{3/2}}. \quad (13)$$

We observe that the structure of ϑ_{d+id} differs substantially to the one in Eq. (11). This concerns both the period for the Friedel oscillations, as well as the dependence on $k_F R$. These differences can be attributed to the Cooper-pairing mechanism which is responsible here for generating the ground state chirality of the substrate.

Figure 3 depicts the evolution of the two susceptibilities along with the arising spin chirality, upon varying the interadatom distance R , in the case of an equilateral triangular configuration. Remarkably, aside from the anticipated spin chirality peaks centered at $\chi = 0$, the spin-singlet pairing promotes the CM state, and renders χ_C nonzero in a substantial portion of the parameter space.

Discussion – From the above, we conclude that our chirality detection protocol is broadly applicable, it can differentiate between normal and superconducting systems and, most importantly, it fully encodes the winding of the Hamiltonian in the Friedel oscillations of the chiral susceptibility. Our approach appears experimentally feasible, since adatom spins can be addressed using scanning tunneling microscopy [59]. Evenmore, the substrate-adatom coupling can be electrically controlled [60–62], while the geometrical details of the setup are also adjustable, thus providing additional control knobs.

Aside from valley-polarized bilayer graphene, our approach appears applicable to magic-angle twisted bilayer graphene, which is known to develop spontaneous Chern phases [63, 64]. Another possibility is the charge-ordered kagomé superconductors [65, 66]. The observed charge-order is theoretically proposed to be a chiral phase [67–69] akin to the one proposed by Haldane [70]. Note that similar to its cousin, i.e., the quantum anomalous Hall state [71, 72], also the charge Chern insulator can be employed for engineering topological superconductivity [73]. Apart from doped Chern insulators, our protocol can be applied to candidate chiral $d + id$ superconductors, such as, SrPtAs [74–76], cuprate bilayers [77] based on Bi-2212 monolayers [78], and intrinsically superconducting graphene when tuned near van Hove singularities [79–82].

NOTE ADDED

At the final stage of completion of this manuscript, we became aware of the preprint in Ref. [83] which has some overlap with our work.

ACKNOWLEDGEMENTS

PK acknowledges funding from the National Natural Science Foundation of China (Grant No. 12250610194).

* huangyupeng@iphy.ac.cn

† kotetes@itp.ac.cn

- [1] A. J. Leggett, *A theoretical description of the new phases of liquid ^3He* , Rev. Mod. Phys. **47**, 331 (1975).
- [2] E. Fradkin, *Field Theories of Condensed Matter Physics*, 2nd Edition (Cambridge University Press, Cambridge, 2013).
- [3] G. E. Volovik, *The Universe in a Helium Droplet* (Oxford University Press, New York, 2003).
- [4] M. König, S. Wiedmann, C. Brüne, Andreas Roth, H. Buhmann, L. W. Molenkamp, X.-L. Qi, and S.-C. Zhang, *Quantum Spin Hall Insulator State in HgTe Quantum Wells*, Science **318**, 766 (2007).
- [5] C.-Z. Chang, J. Zhang, X. Feng, J. Shen, Z. Zhang, M. Guo, K. Li, Y. Ou, P. Wei, L.-L. Wang, Z.-Q. Ji, Y. Feng, S. Ji, X. Chen, J. Jia, X. Dai, Z. Fang, S.-C. Zhang, K. He, Y. Wang, L. Lu, X.-C. Ma, and Q.-K. Xue, *Experimental Observation of the Quantum Anomalous Hall Effect in a Magnetic Topological Insulator*, Science **340**, 167 (2013).
- [6] Q. L. He, L. Pan, A. L. Stern, E. C. Burks, X. Che, G. Yin, J. Wang, B. Lian, Q. Zhou, E. Sang Choi, K. Murata, X. Kou, Z. Chen T. Nie, Q. Shao, Y. Fan, S.-C. Zhang, K. Liu, J. Xia, and K. L. Wang, *RETRACTED: Chiral Majorana fermion modes in a quantum anomalous Hall insulator-superconductor structure*, Science **357**, 294 (2017).
- [7] M. Kayyalha, D. Xiao, R. Zhang, J. Shin, J. Jiang, F. Wang, Y.-F. Zhao, R. Xiao, L. Zhang, K. M. Fijalkowski, P. Mandal, M. Winnerlein, C. Gould, Q. Li, L. W. Molenkamp, M. H. W. Chan, N. Samarth, and C.-Z. Chang, *Absence of evidence for chiral Majorana modes in quantum anomalous Hall-superconductor devices*, Science **367**, 64 (2020).
- [8] D. Xiao, M.-C. Chang, and Q. Niu, *Berry phase effects on electronic properties*, Rev. Mod. Phys. **82**, 1959 (2010).
- [9] P. Kotetes, *Topological Insulators* (Morgan & Claypool, San Rafael, USA, 2019).
- [10] H. S. Bennett and E. A. Stern, *Faraday Effect in Solids*, Phys. Rev. **137**, A448 (1965).
- [11] A. Kapitulnik, J. Xia, E. Schemm, and A. Palevski, *Polar Kerr effect as probe for time-reversal symmetry breaking in unconventional superconductors*, New J. Phys. **11**, 055060 (2009).
- [12] J. Xia, Y. Maeno, P. T. Beyersdorf, M. M. Fejer, and A. Kapitulnik, *High Resolution Polar Kerr Effect Measurements of Sr_2RuO_4 : Evidence for Broken Time-Reversal Symmetry in the Superconducting State*, Phys. Rev. Lett. **97**, 167002 (2006).
- [13] Y. Maeno, S. Yonezawa, and A. Ramires, *Still mystery after all these years - Unconventional superconductivity of Sr_2RuO_4* , arXiv:2402.12117.
- [14] J. Villain, *Spin glass with non-random interactions*, J. Phys. C **10**, 1717 (1977); *Two-level systems in a spin-glass model. I. General formalism and two-dimensional model*, *ibid* **10**, 4793 (1977).
- [15] S. Miyashita and H. Shiba, *Nature of the Phase Transition of the Two-Dimensional Antiferromagnetic Plane Rotator Model on the Triangular Lattice*, J. Phys. Soc. Jpn. **53**, 1145 (1984).
- [16] X. G. Wen, F. Wilczek, and A. Zee *Chiral spin states and superconductivity*, Phys. Rev. B **39**, 11413 (1989).
- [17] M. A. Ruderman and C. Kittel, *Indirect Exchange Coupling of Nuclear Magnetic Moments by Conduction Electrons*, Phys. Rev. **96**, 99 (1954); T. Kasuya, *A Theory of Metallic Ferro- and Antiferromagnetism on Zener's Model*, Progr. Theor. Phys., **16**, 45 (1956); K. Yosida, *Magnetic Properties of Cu-Mn Alloys*, Phys. Rev. **106**, 893 (1957).
- [18] A. V. Balatsky, I. Vekhter, and J.-X. Zhu, *Impurity-induced states in conventional and unconventional superconductors*, Rev. Mod. Phys. **78**, 373 (2006).
- [19] I. Martin and C. D. Batista, *Itinerant Electron-Driven Chiral Magnetic Ordering and Spontaneous Quantum Hall Effect in Triangular Lattice Models*, Phys. Rev. Lett. **101**, 156402 (2008).
- [20] Y. Akagi, M. Udagawa, and Y. Motome, *Hidden Multiple-Spin Interactions as an Origin of Spin Scalar Chiral Order in Frustrated Kondo Lattice Models*, Phys. Rev. Lett. **108**, 096401 (2012).
- [21] S. Hayami and Y. Motome, *Topological spin crystals by itinerant frustration*, J. Phys.: Condens. Matter **33**, 443001 (2021).
- [22] C. Hickey, L. Cincio, Z. Papić, and A. Paramekanti, *Emergence of chiral spin liquids via quantum melting of noncoplanar magnetic orders*, Phys. Rev. B **96**, 115115 (2017).
- [23] Y.-F. Jiang and H.-C. Jiang, *Topological Superconductivity in the Doped Chiral Spin Liquid on the Triangular Lattice*, Phys. Rev. Lett. **125**, 157002 (2020).

- [24] Y. Huang and D. N. Sheng, *Topological Chiral and Nematic Superconductivity by Doping Mott Insulators on Triangular Lattice*, Phys. Rev. X **12**, 031009 (2022).
- [25] A. Bose, A. Haldar, E. S. Sørensen, and A. Paramekanti, *Chiral Broken Symmetry Descendants of the Kagomé Lattice Chiral Spin Liquid*, Phys. Rev. B **107**, L020411 (2023).
- [26] D. Sen and R. Chitra, *Large- U limit of a Hubbard model in a magnetic field: Chiral spin interactions and paramagnetism*, Phys. Rev. B **51**, 1922 (1995).
- [27] V. W. Scarola, K. Park, and S. Das Sarma, *Chirality in Quantum Computation with Spin Cluster Qubits*, Phys. Rev. Lett. **93**, 120503 (2004).
- [28] Z. Dong and L. Levitov, *Chiral Stoner Magnetism in Dirac Bands, Chiral Stoner magnetism in dirac bands*, arXiv:2208.02051.
- [29] Y.-P. Huang and P. Kotetes, *Mechanisms for magnetic skyrmion catalysis and topological superconductivity*, Phys. Rev. Research **5**, 013125 (2023).
- [30] P. Kotetes and Y.-P. Huang, *New mechanisms to engineer magnetic skyrmions and topological superconductors*, Proc. SPIE 12656, Spintronics XVI, 126560T (28 September 2023).
- [31] See Supplemental Material at [url] for additional technical details regarding the general exploration of the possible magnetic ground states, and the calculation of the effective spin interactions for (i) a single valley of bilayer graphene and (ii) a spin-singlet $d + id$ superconductor.
- [32] J. Lorenzana, G. Seibold, C. Ortix, and M. Grilli, *Competing Orders in FeAs Layers*, Phys. Rev. Lett. **101**, 186402 (2008).
- [33] M. H. Christensen, B. M. Andersen, and P. Kotetes, *Unravelling Incommensurate Magnetism and Its Emergence in Iron-Based Superconductors* Phys. Rev. X **8**, 041022 (2018).
- [34] S. Hayami, R. Ozawa, and Y. Motome, *Engineering chiral density waves and topological band structures by multiple- Q superpositions of collinear up-up-down-down orders*, Phys. Rev. B **94**, 024424 (2016).
- [35] Y.-P. Huang, J.-W. Dong, P. Kotetes, and S. Zhou, *Antiferromagnetic chiral spin density wave and strain-induced Chern insulator in the square lattice Hubbard model with frustration*, Phys. Rev. B **102**, 195120 (2020).
- [36] L. Fu, *Topological Crystalline Insulators*, Phys. Rev. Lett. **106**, 106802 (2011).
- [37] J.-X. Zhu and A. V. Balatsky, *Field induced $d_{x^2-y^2} + id_{xy}$ state in d -density-wave metals*, Phys. Rev. B **65**, 132502 (2002).
- [38] S. Raghu, X.-L. Qi, C. Honerkamp, and S.-C. Zhang, *Topological Mott Insulators*, Phys. Rev. Lett. **100**, 156401 (2008).
- [39] S. Tewari, C. Zhang, V. M. Yakovenko, and S. Das Sarma, *Time-reversal symmetry breaking by a $(d+id)$ density-wave state in underdoped cuprate superconductors*, Phys. Rev. Lett. **100**, 217004 (2008).
- [40] P. Kotetes and G. Varelogiannis, *Meissner effect without superconductivity from a chiral d -density wave*, Phys. Rev. B **78**, 220509(R) (2008).
- [41] C. Zhang, S. Tewari, V. M. Yakovenko, and S. Das Sarma, *Anomalous Nernst effect from a chiral d -density-wave state in underdoped cuprate superconductors*, Phys. Rev. B **78**, 174508 (2008).
- [42] P. Kotetes and G. Varelogiannis, *Chirality Induced Tilted-Hill Giant Nernst Signal*, Phys. Rev. Lett. **104**, 106404 (2010).
- [43] J. W. F. Venderbos, *Symmetry analysis of translational symmetry broken density waves: Application to hexagonal lattices in two dimensions*, Phys. Rev. B **93**, 115107 (2016).
- [44] E. McCann and F. Fal'ko, *Landau-Level Degeneracy and Quantum Hall Effect in a Graphite Bilayer*, Phys. Rev. Lett. **96**, 086805 (2006).
- [45] D. Xiao, W. Yao, and Q. Niu, *Valley-Contrasting Physics in Graphene: Magnetic Moment and Topological Transport*, Phys. Rev. Lett. **99**, 236809 (2007).
- [46] M. Sui, G. Chen, L. Ma, W.-Y. Shan, D. Tian, K. Watanabe, T. Taniguchi, X. Jin, W. Yao, D. Xiao, and Y. Zhang, *Gate-tunable topological valley transport in bilayer graphene*, Nat. Phys. **11**, 1027 (2015).
- [47] Y. Shimazaki, M. Yamamoto, I. V. Borzenets, K. Watanabe, T. Taniguchi, and S. Tarucha, *Generation and detection of pure valley current by electrically induced Berry curvature in bilayer graphene*, Nat. Phys. **11**, 1032 (2015).
- [48] H. Chen, P. Zhou, J. Liu. et al., *Gate controlled valley polarizer in bilayer graphene*, Nat Commun. **11**, 1202 (2020).
- [49] E. H. Hwang and S. Das Sarma, *Screening, Kohn Anomaly, Friedel Oscillation, and RKKY Interaction in Bilayer Graphene*, Phys. Rev. Lett. **101**, 156802 (2008).
- [50] A. H. Castro Neto, F. Guinea, N. M. R. Peres, K. S. Novoselov, and A. K. Geim, *The electronic properties of graphene*, Rev. Mod. Phys. **81**, 109 (2009).
- [51] M. Sherafati and S. Satpathy, *RKKY interaction in graphene from the lattice Green's function*, Phys. Rev. B **83**, 165425 (2011).
- [52] F. Parhizgar, M. Sherafati, R. Asgari, and S. Satpathy, *Ruderman-Kittel-Kasuya-Yosida interaction in biased bilayer graphene*, Phys. Rev. B **87**, 165429 (2013).
- [53] A. Allerdt, A. E. Feiguin, and S. Das Sarma, *Competition between Kondo effect and RKKY physics in graphene magnetism*, Phys. Rev. B **95**, 104402 (2017).
- [54] R. B. Laughlin, *Magnetic Induction of $d_{x^2-y^2} + id_{xy}$ Order in High- T_c Superconductors*, Phys. Rev. Lett. **80**, 5188 (1998).
- [55] D. N. Aristov, S.V. Maleyev and A.G. Yashenkin, *RKKY interaction in layered superconductors with anisotropic pairing*, Z. Phys. B: Condens. Matter **102**, 467 (1997).
- [56] N. Y. Yao, L. I. Glazman, E. A. Demler, M. D. Lukin, and J. D. Sau, *Enhanced Antiferromagnetic Exchange between Magnetic Impurities in a Superconducting Host*, Phys. Rev. Lett. **113**, 087202 (2014).
- [57] M. Schechter, K. Flensberg, M. H. Christensen, B. M. Andersen, and J. Paaske, *Self-organized topological superconductivity in a Yu-Shiba-Rusinov chain*, Phys. Rev. B **93**, 140503 (2016).
- [58] M. Schechter, O. F. Syljuåsen, and J. Paaske, *Cooper pair induced frustration and nematicity of two-dimensional magnetic adatom lattices*, Phys. Rev. B **97**, 174412 (2018).
- [59] R. Wiesendanger, *Spin mapping at the nanoscale and atomic scale*, Rev. Mod. Phys. **81**, 1495 (2009).
- [60] D. Nafday and T. Saha-Dasgupta, *Magnetism of an adatom on bilayer graphene and its control: A first-principles perspective*, Phys. Rev. B **88**, 205422 (2013).
- [61] D. Nafday, M. Kabir, and T. Saha-Dasgupta, *Controlling adatom magnetism on bilayer graphene by external field*, Phys. Rev. B **93**, 045433 (2016).

- [62] M. Killi, D. Heidarian and A. Paramekanti, *Controlling local moment formation and local moment interactions in bilayer graphene*, New J. Phys. **13**, 053043 (2011).
- [63] M. Serlin, C. L. Tschirhart, H. Polshyn, Y. Zhang, J. Zhu, K. Watanabe, T. Taniguchi, L. Balents, and A. F. Young, *Intrinsic quantized anomalous Hall effect in a moiré heterostructure*, Science **367**, 900 (2020).
- [64] K. P. Nuckolls, M. Oh, D. Wong, B. Lian, K. Watanabe, T. Taniguchi, B. A. Bernevig, and A. Yazdani, *Strongly correlated Chern insulators in magic-angle twisted bilayer graphene*, Nature (London) **588**, 610 (2020).
- [65] Y.-X. Jiang, J.-X. Yin, M. M. Denner, N. Shumiya, B. R. Ortiz, G. Xu, Z. Guguchia, J. He, Md S. Hossain, X. Liu, J. Ruff, L. Kautzsch, S. S. Zhang, G. Chang, I. Belopolski, Q. Zhang, T. A. Cochran, D. Multer, M. Litskevich, Z.-J. Cheng, X. P. Yang, Z. Wang, R. Thomale, T. Neupert, S. D. Wilson, and M. Zahid Hasan, *Unconventional chiral charge order in kagome superconductor KV_3Sb_5* , Nat. Mater. **20**, 1353 (2021).
- [66] H. Zhao, H. Li, B. R. Ortiz, S. M. L. Teicher, T. Park, M. Ye, Z. Wang, L. Balents, S. D. Wilson, and I. Zeljkovic, *Cascade of correlated electron states in a kagome superconductor CsV_3Sb_5* , Nature (London) **599**, 216 (2021).
- [67] X. Feng, K. Jiang, Z. Wang, and J. Hu, *Chiral flux phase in the kagome superconductor AV_3Sb_5* , Sci. Bull. **66**, 1384 (2021).
- [68] X. Feng, Y. Zhang, K. Jiang, and J. Hu, *Low-energy effective theory and symmetry classification of flux phases on Kagome lattice*, Phys. Rev. B **104**, 165136 (2021).
- [69] Y.-P. Lin and R. M. Nandkishore, *Complex charge density waves at Van Hove singularity on hexagonal lattices: Haldane-model phase diagram and potential realization in kagome metals AV_3Sb_5* , Phys. Rev. B **104**, 045122 (2021).
- [70] F. D. M. Haldane, *Model for a Quantum Hall Effect Without Landau Levels: Condensed-matter Realization of the Parity Anomaly*, Phys. Rev. Lett. **61**, 2015 (1988).
- [71] X.-L. Qi, T. L. Hughes, and S.-C. Zhang, *Chiral topological superconductor from the quantum Hall state*, Phys. Rev. B **82**, 184516 (2010).
- [72] C.-Z. Chen, Y.-M. Xie, J. Liu, P. A. Lee, and K. T. Law, *Quasi-one-dimensional quantum anomalous Hall systems as new platforms for scalable topological quantum computation*, Phys. Rev. B **97**, 104504 (2018).
- [73] J.-A. Wang, S. Zhou, and P. Kotetes, *Majorana braiding racetracks from charge Chern insulator-superconductor hybrids*, Phys. Rev. B **105**, 045423 (2022).
- [74] Y. Nishikubo, K. Kudo, and M. Nohara, *Superconductivity in the Honeycomb-Lattice Pnictide $SrPtAs$* , J. Phys. Soc. Jpn. **80**, 055002 (2011).
- [75] P. K. Biswas, H. Luetkens, T. Neupert, T. Stürzer, C. Baines, G. Pascua, A. P. Schnyder, M. H. Fischer, J. Goryo, M. R. Lees, H. Maeter, F. Brückner, H.-H. Klauss, M. Nicklas, P. J. Baker, A. D. Hillier, M. Sigrist, A. Amato, and D. Johrendt, *Evidence for superconductivity with broken time-reversal symmetry in locally noncentrosymmetric $SrPtAs$* , Phys. Rev. B **87**, 180503(R) (2013).
- [76] M. H. Fischer, T. Neupert, C. Platt, A. P. Schnyder, W. Hanke, J. Goryo, R. Thomale, and M. Sigrist, *Chiral d -wave superconductivity in $SrPtAs$* Phys. Rev. B **89**, 020509(R) (2014).
- [77] O. Can, T. Tummuru, R. P. Day, I. Elfimov, A. Damascelli, and M. Franz, *High-temperature topological superconductivity in twisted double-layer copper oxides*, Nat. Phys. **17**, 519 (2021).
- [78] Y. Yu, L. Ma, P. Cai, R. Zhong, C. Ye, J. Shen, G D. Gu, X.-H. Chen, and Y. Zhang, *High-temperature superconductivity in monolayer $Bi_2Sr_2CaCu_2O_{8+\delta}$* , Nature **575**, 156 (2019).
- [79] A. M. Black-Schaffer and S. Doniach, *Resonating valence bonds and mean-field d -wave superconductivity in graphite*, Phys. Rev. B **75**, 134512 (2007).
- [80] S. Pathak, V. B. Shenoy, and G. Baskaran, *Possible high-temperature superconducting state with a $d + id$ pairing symmetry in doped graphene*, Phys. Rev. B **81**, 085431 (2010).
- [81] R. Nandkishore, L. S. Levitov, and A. V. Chubukov, *Chiral superconductivity from repulsive interactions in doped graphene*, Nat. Phys. **8**, 158 (2012).
- [82] M. L. Kiesel, C. Platt, W. Hanke, D. A. Abanin, and R. Thomale, *Competing many-body instabilities and unconventional superconductivity in graphene*, Phys. Rev. B **86**, 020507(R) (2012).
- [83] A. Panigrahi, V. Poliakov, Z. Dong, and L. Levitov, *Spin chirality and fermion stirring in topological bands*, arXiv:2407.17433.

Supplemental Material

Imprinting Ground State Chirality on Adatom Spins

Yun-Peng Huang¹ and Panagiotis Kotetes²

¹ Beijing National Laboratory for Condensed Matter Physics, and Institute of Physics, Chinese Academy of Sciences, Beijing 100190, China

² CAS Key Laboratory of Theoretical Physics, Institute of Theoretical Physics, Chinese Academy of Sciences, Beijing 100190, China

A. Magnetic Ground States

We base our analysis on the effective chiral Heisenberg spin model of the main text. We choose to parametrize the spins of the three adatoms in the following fashion $\mathbf{S}_1 = (0, 0, 1)$, $\mathbf{S}_2 = (0, \sin \phi, \cos \phi)$, and $\mathbf{S}_3 = (\sin \omega \sin \eta, \sin \omega \cos \eta, \cos \omega)$, where $\phi \in [0, 2\pi)$, $\omega \in [0, \pi]$, and $\eta \in [0, 2\pi)$. After replacing the spins in terms of the angles (ϕ, ω, η) , we find the energy functional:

$$E_{\text{spins}} = -J^2 [\chi_{12} \cos \phi + \chi_{13} \cos \omega + \chi_{23} \cos \phi \cos \omega + \sin \phi \sin \omega (\chi_{23} \cos \eta - J\vartheta \sin \eta)]. \quad (14)$$

We proceed by extremizing the functional. We first extremize with respect to η , i.e., $\partial E_{\text{spins}}/\partial \eta = 0$, and find:

$$\sin \phi \sin \omega (\chi_{23} \sin \eta + J\vartheta \cos \eta) = 0, \quad (15)$$

which leads to the following possibilities:

- $\phi = \{0, \pi\}$. In these cases \mathbf{S}_1 and \mathbf{S}_2 are collinear. Further extremization with respect to ω yields the two subcases $\omega = \{0, \pi\}$. Therefore, in this case all the spins are collinear and there exist two possible ground states, the ferromagnetic (FM) and the here-termed frustrated FM (FFM). In the latter, one of the three spins which are aligned in the FM state flips direction. The energy for the FM alignment is given by $E_{\text{FM}} = -J^2(\chi_{12} + \chi_{13} + \chi_{23})$. In contrast, for the FFM scenario we find three nonequivalent possibilities when $\chi_{12} \neq \chi_{13} \neq \chi_{23}$. Hence, depending on which spin is flipped, we find $E_{\text{FFM}}^{\uparrow\uparrow\downarrow} = -J^2(\chi_{12} - \chi_{13} - \chi_{23})$, $E_{\text{FFM}}^{\uparrow\downarrow\uparrow} = -J^2(\chi_{13} - \chi_{12} - \chi_{23})$, and $E_{\text{FFM}}^{\downarrow\uparrow\uparrow} = -J^2(\chi_{23} - \chi_{12} - \chi_{13})$.
- $\omega = \{0, \pi\}$. Due to the arising symmetry of the energy functional under the exchange $\phi \leftrightarrow \omega$, this and the previous case lead to the same ground states.
- $\vartheta \neq 0$ and $\tan \eta = -J\vartheta/\chi_{23}$. This corresponds to the noncoplanar chiral ground state. By making use of this relation, we find that the energy now becomes:

$$E_{\text{spins}} = -J^2 \left[\chi_{12} \cos \phi + \chi_{13} \cos \omega + \chi_{23} \cos \phi \cos \omega - \text{sgn}(J\vartheta \sin \eta) \sqrt{\chi_{23}^2 + (J\vartheta)^2} \sin \phi \sin \omega \right]. \quad (16)$$

We proceed by further extremizing with respect to ω and find the condition:

$$\tan \omega = -\frac{\text{sgn}(J\vartheta \sin \eta) \sqrt{\chi_{23}^2 + (J\vartheta)^2} \sin \phi}{\chi_{13} + \chi_{23} \cos \phi}. \quad (17)$$

By making use of the above relation, we obtain the following form of the energy functional at this extremum:

$$E_{\text{spins}} = -J^2 \left\{ \chi_{12} \cos \phi - \text{sgn}(J\vartheta \sin \eta \sin \phi) \sqrt{(\chi_{13} + \chi_{23} \cos \phi)^2 + [\chi_{23}^2 + (J\vartheta)^2] \sin^2 \phi} \right\}. \quad (18)$$

We remind the reader that since $\phi \neq \{0, \pi\}$ the function $\sin \phi$ is nonzero. Thus, we can proceed with the extremization in terms of ϕ by separately considering the two cases depending on the value of $\text{sgn}(\sin \phi)$. By extremizing with respect to ϕ in each case, we find:

$$\chi_{12} = \text{sgn}(J\vartheta \sin \eta \sin \phi) \frac{\chi_{13}\chi_{23} - (J\vartheta)^2 \cos \phi}{\sqrt{(\chi_{13} + \chi_{23} \cos \phi)^2 + [\chi_{23}^2 + (J\vartheta)^2] \sin^2 \phi}}, \quad (19)$$

and after solving for $\cos \phi$, we find the two possible solutions:

$$\frac{[\chi_{12}^2 + (J\vartheta)^2] \cos \phi - \chi_{13}\chi_{23}}{\chi_{12}} = \frac{\chi_{12}\chi_{13}\chi_{23} \pm \sqrt{[\chi_{12}^2 + (J\vartheta)^2][\chi_{13}^2 + (J\vartheta)^2][\chi_{23}^2 + (J\vartheta)^2]}}{(J\vartheta)^2}, \quad (20)$$

which results in the ground state energy of the chiral magnetic state:

$$E_{\text{CM}} = -\frac{|\chi_{12}\chi_{13}\chi_{23}|}{\vartheta^2} \left\{ \text{sgn}(\chi_{12}\chi_{13}\chi_{23}) \pm \sqrt{\left[1 + \left(\frac{J\vartheta}{\chi_{12}}\right)^2\right] \left[1 + \left(\frac{J\vartheta}{\chi_{13}}\right)^2\right] \left[1 + \left(\frac{J\vartheta}{\chi_{23}}\right)^2\right]} \right\}. \quad (21)$$

The above sign ambiguity is resolved by choosing the solution for $\cos \phi$ which minimizes the energy. Since the term under the square root is larger than one, we find that independent of the sign of $\chi_{12}\chi_{13}\chi_{23}$ the “+” solution minimizes the energy. Hence, one can now trace the steps backwards and identify the various parameters.

- $\vartheta = 0$ and $\eta = \{0, \pi\}$. This state corresponds to the coplanar here-termed spin flux (SF) state. Given these conditions the energy functional takes the form below:

$$E_{\text{spins}} = -J^2 (\chi_{12} \cos \phi + \chi_{13} \cos \omega + \chi_{23} \cos \phi \cos \omega + e^{i\eta} \chi_{23} \sin \phi \sin \omega). \quad (22)$$

Extremizing with respect to ω leads to the condition:

$$\tan \omega = \frac{e^{i\eta} \chi_{23} \sin \phi}{\chi_{13} + \chi_{23} \cos \phi}, \quad (23)$$

which allows us to write the energy of this extremum as follows:

$$E_{\text{spins}} = -J^2 \left[\chi_{12} \cos \phi + e^{i\eta} \text{sgn}(\chi_{23} \sin \phi) \sqrt{(\chi_{13} + \chi_{23} \cos \phi)^2 + (\chi_{23} \sin \phi)^2} \right]. \quad (24)$$

In the same spirit with the process followed in the previous paragraph for the CM state, here extremizing yields:

$$\chi_{12} = -e^{i\eta} \text{sgn}(\chi_{23} \sin \phi) \frac{\chi_{13} \chi_{23}}{\sqrt{(\chi_{13} + \chi_{23} \cos \phi)^2 + (\chi_{23} \sin \phi)^2}}, \quad (25)$$

as well as the solution:

$$\chi_{12}^2 \cos \phi - \chi_{13} \chi_{23} = -\frac{(\chi_{12} \chi_{13})^2 + (\chi_{12} \chi_{23})^2 + (\chi_{13} \chi_{23})^2}{2\chi_{13} \chi_{23}}. \quad (26)$$

Using the above, we find the energy of this ground state:

$$E_{\text{SF}} = J^2 \frac{(\chi_{12} \chi_{13})^2 + (\chi_{12} \chi_{23})^2 + (\chi_{13} \chi_{23})^2}{2\chi_{12} \chi_{13} \chi_{23}}. \quad (27)$$

Before proceeding, we examine how the above results for the four distinct magnetic states simplify when the adatoms form an equilateral triangle, where $\chi_{12,13,23} \equiv \chi$.

- FM state. The energy becomes $E_{\text{FM}} = -3J^2\chi$.
- FFM state. The energy in this case is given by $E_{\text{FFM}} = J^2\chi$.
- SF state. Here, we find $E_{\text{SF}} = 3J^2\chi/2$. When $\vartheta = 0$ and $\chi < 0$, the SF is stabilized as the ground state. By choosing $\eta = \pi$ with no loss of generality, we find $\phi = \omega = 2\pi/3$. Thus, successive spins form an angle of $2\pi/3$.
- CM state. In this case the energy becomes:

$$E_{\text{CM}} = -J^2\chi \frac{1 + \text{sgn}(\chi) \sqrt{1 + (J\vartheta/\chi)^2}^3}{(J\vartheta/\chi)^2}, \quad (28)$$

while $\cos \phi$ is to be determined by the following relation:

$$\cos \phi = \frac{1}{1 + (J\vartheta/\chi)^2} \left[1 + \frac{1 + \text{sgn}(\chi) \sqrt{1 + (J\vartheta/\chi)^2}^3}{(J\vartheta/\chi)^2} \right]. \quad (29)$$

We investigate the competition of the CM state and the collinear ones for the two signs of χ .

- $\chi > 0$. Here, the CM competes with FM. We find that $\cos \phi$ does not have a solution for $|J\vartheta| < \sqrt{3}\chi$, while $\cos \phi \in [0, 1]$ for $|J\vartheta| \geq \sqrt{3}\chi$. Note that $\cos \phi = 1$ ($\cos \phi = 0$) for $|J\vartheta| = \sqrt{3}\chi$ ($|J\vartheta|/\chi \rightarrow \infty$). Interestingly, in the same interval that the CM state is well-defined, it also becomes the ground state, with its energy being exactly equal to $E_{\text{FM}} = -3J^2\chi$ at $|J\vartheta| = \sqrt{3}\chi$, and further decreasing upon increasing $|J\vartheta|/\chi$ beyond the value $\sqrt{3}$. Hence, we observe that a critical strength of $|J\vartheta|/\chi$ is required to induce spin chirality on the adatom spins.

- (ii) $\chi = -|\chi| < 0$. In this parameter regime, there always exist a CM solution. Specifically, we find that $\cos\phi \in [-1/2, 0)$, with the minimum (maximum) value obtained for $|J\vartheta/\chi| = 0$ ($|J\vartheta/\chi| \rightarrow \infty$). Quite remarkably, for $\chi < 0$ the limit $\vartheta \rightarrow 0$ is well-defined and the CM state energy becomes equal to $-3J^2|\chi|/2$. Hence, the CM state evolves into the SF state, thus, implying that SF and CM states are adiabatically connected and constitute the ground states of the adatom complex for $\chi < 0$. Finally, we conclude that the FFM state never becomes the ground state solution.

B. Calculations for Bilayer Graphene

In this section, we provide further details on obtaining the RKKY and chiral susceptibilities via the Euclidean Green function approach.

I. Model Hamiltonian

We formally bring the BG Hamiltonian $\hat{H}(\mathbf{k})$ into a diagonal form by expressing it as $\hat{H}(\mathbf{k}) = \sum_{\alpha=\pm} \varepsilon_{\alpha}(\mathbf{k}) \hat{P}_{\alpha}(\mathbf{k})$, where we have introduced the projectors $\hat{P}_{\alpha}(\mathbf{k}) = [\hat{1} + \alpha \hat{\mathbf{d}}(\mathbf{k}) \cdot \boldsymbol{\tau}] / 2$ and the unit vector $\hat{\mathbf{d}}(\mathbf{k}) = \mathbf{d}(\mathbf{k}) / |\mathbf{d}(\mathbf{k})|$. These projectors correspond to the energy dispersions $\varepsilon_{\alpha}(\mathbf{k}) = \alpha |\mathbf{d}(\mathbf{k})| - \mu \equiv \varepsilon_{\alpha}(k)$, where $k = |\mathbf{k}|$. Here, we have $|\mathbf{d}(\mathbf{k})|^2 = \Delta^2 (k/k_0)^4 + V^2 [(k/k_0)^2 - 1]^2$. Straightforward algebra yields that $|\mathbf{d}(\mathbf{k})|$ has a local maximum at $k = 0$ with $|\mathbf{d}(\mathbf{k})|_{\text{local max}} = |V|$, while it reaches its global minimum for $k = k_0 |V| / \sqrt{\Delta^2 + V^2}$ with $|\mathbf{d}(\mathbf{k})|_{\text{global min}} = |V\Delta| / \sqrt{\Delta^2 + V^2} \equiv E_{\text{min}}$. When $|V| \ll |\Delta|$ we find that $E_{\text{min}} \rightarrow |V|$ and the two extrema coincide. From the above, we conclude that in order to obtain a Fermi surface, the chemical potential should satisfy $|\mu| > E_{\text{min}}$, while the given model is valid in the interval $10^{-2} \leq E_F / |\Delta| \leq 2$. This is because $\Delta = \gamma_1 / 2$ and $k_0 = \gamma_1 / \sqrt{2} \hbar v_g$, where $\gamma_1 = 390 \text{ meV}$ and $v_g \simeq 8 \cdot 10^5 \text{ m/s}$. In the following, we focus on the case $\mu = E_F > 0$, and find that only the $\varepsilon_+(\mathbf{k})$ band leads to a Fermi surface, with a Fermi wavenumber:

$$\left(\frac{k_F}{k_0}\right)^2 = \frac{E_{\text{min}}}{\sqrt{\Delta^2 + V^2}} \left[\left| \frac{V}{\Delta} \right| + \sqrt{\left(\frac{E_F}{E_{\text{min}}}\right)^2 - 1} \right], \quad (30)$$

since we have $|\Delta| > |V|$. Note that when $|\Delta| \gg |V|$ and $E_F \simeq |\Delta|$, we have $k_F \simeq k_0$. In the remainder we consider that E_F is substantially larger than $|V|$, so that it gives rise to a sufficiently large Fermi pocket which dominates the RKKY and chiral interactions. Hence, under these assumptions, we can completely neglect the gapped dispersion $\varepsilon_-(k)$. In contrast, we keep the dispersion $\varepsilon_+(k)$ and additionally linearize it about the Fermi wavenumber. This procedure yields the result:

$$\varepsilon_+(k) = \frac{2k_F}{E_F k_0^2} \sqrt{(\Delta^2 + V^2) E_F^2 - (V\Delta)^2} (k - k_F). \quad (31)$$

II. Coordinate-Space Matrix Green Function

Under the single-dispersion approximation discussed in the previous paragraph, the reciprocal space matrix Green function is expressed as $\hat{G}(\varepsilon, \mathbf{k}) = \sum_{\alpha=\pm} [\imath\varepsilon - \varepsilon_{\alpha}(k)]^{-1} \hat{P}_{\alpha}(\mathbf{k}) \approx [\imath\varepsilon - \varepsilon_+(k)]^{-1} \hat{P}_+(\mathbf{k})$. We now proceed and evaluate the coordinate-space matrix Green function $\hat{G}(\varepsilon, \mathbf{R})$ by means of a Fourier transform. By setting $\mathbf{k} = k(\cos\varphi, \sin\varphi)$ and $\mathbf{R} = R(\cos\theta, \sin\theta)$, we have $\mathbf{k} \cdot \mathbf{R} = kR \cos(\varphi - \theta)$. We introduce the dimensionless parameter $u = k_F/k_0$ and obtain the following expression for the coordinate-space matrix Green function for $k \approx k_F$:

$$\hat{G}(\varepsilon, \mathbf{R}) \approx \int_0^{\infty} \frac{dk k_F}{2\pi} \int_{-\pi}^{+\pi} \frac{d\varphi}{2\pi} \frac{e^{\imath k R \cos(\varphi - \theta)}}{\imath\varepsilon - \varepsilon_+(k)} \frac{E_F + \Delta u^2 \cos(2\varphi)\tau_1 + \Delta u^2 \sin(2\varphi)\tau_2 + V(u^2 - 1)\tau_3}{2E_F}. \quad (32)$$

We now employ the integral definition of the ordinary Bessel functions of the first kind:

$$\imath^n J_n(z) = \int_{-\pi}^{+\pi} \frac{d\varphi}{2\pi} e^{\imath z \cos\varphi} \cos(n\varphi) \quad (33)$$

and carry out the integration over the angle entering in the formula for the matrix Green function. This provides:

$$\hat{G}(\varepsilon, \mathbf{R}) = \int_0^\infty \frac{dk k_F}{2\pi} \frac{1}{i\varepsilon - \varepsilon_+(k)} \frac{[E_F + V(u^2 - 1)\tau_3]J_0(kR) - \Delta u^2 [\cos(2\theta)\tau_1 + \sin(2\theta)\tau_2]J_2(kR)}{2E_F}. \quad (34)$$

The next step is to integrate out the radial wavenumber part. We consider the case where the adatoms distance R is much larger than the Fermi wavelength $\lambda_F = 2\pi/k_F$. Given this assumption, we employ the following approximate forms $J_n(z) \approx \sqrt{2/(\pi z)} \cos(z - \pi/4 - n\pi/2)$ and find the expression:

$$\hat{G}(\varepsilon, \mathbf{R}) \approx \sqrt{\frac{2}{\pi k_F R}} \frac{E_F + V(u^2 - 1)\tau_3 + \Delta u^2 [\cos(2\theta)\tau_1 + \sin(2\theta)\tau_2]}{2E_F} \int_0^\infty \frac{dk k_F}{2\pi} \frac{\cos(kR - \frac{\pi}{4})}{i\varepsilon - \varepsilon_+(k)}. \quad (35)$$

We evaluate the integral above by employing the linearized form of the dispersion $\varepsilon_+(k)$ and by considering the quasi-classical $E_F \rightarrow \infty$ we write:

$$\int_0^\infty \frac{dk k_F}{2\pi} \frac{\cos(kR - \frac{\pi}{4})}{i\varepsilon - \varepsilon_+(k)} \approx -\nu_F \int_{-\infty}^{+\infty} d\xi \frac{\cos(k_F R - \frac{\pi}{4} + \frac{\xi R}{\hbar v_F})}{\xi - i\varepsilon} = -i \text{sgn}(\varepsilon) \pi \nu_F e^{i \text{sgn}(\varepsilon)(k_F R - \frac{\pi}{4}) - \frac{|\varepsilon| R}{\hbar v_F}}, \quad (36)$$

where we introduced the density of states at the Fermi level:

$$\nu_F = \frac{k_0^2}{4\pi} \frac{E_F}{\sqrt{(\Delta^2 + V^2)E_F^2 - (V\Delta)^2}}, \quad (37)$$

along with the Fermi velocity $v_F = k_F/2\pi\hbar\nu_F$. Hence, we conclude with the final expression of the coordinate-space matrix Green function:

$$\hat{G}(\varepsilon, R, \theta) = \frac{-i \text{sgn}(\varepsilon) \pi \nu_F}{\sqrt{2\pi k_F R}} \frac{E_F + V(u^2 - 1)\tau_3 + \Delta u^2 [\cos(2\theta)\tau_1 + \sin(2\theta)\tau_2]}{E_F} \text{Exp} \left[i \text{sgn}(\varepsilon) \left(k_F R - \frac{\pi}{4} \right) - \frac{|\varepsilon| R}{\hbar v_F} \right]. \quad (38)$$

III. RKKY and Chiral Susceptibilities

We now make use of the above result to find the coefficient of the RKKY term. It is straightforward to obtain:

$$\chi(R) = -2 \int_{-\infty}^{+\infty} \frac{d\varepsilon}{2\pi} \text{tr} \left[\hat{G}(\varepsilon, R, \theta) \hat{G}(\varepsilon, R, \theta + \pi) \right] = \frac{\nu_F}{\pi R^2} \sin(2k_F R). \quad (39)$$

We follow the same approach in order to calculate the chiral susceptibility. For this purpose, we introduce the vectors $\mathbf{R}_{ij} = R_1(\cos \theta_1, \sin \theta_1)$, $\mathbf{R}_{jk} = R_2(\cos \theta_2, \sin \theta_2)$, and $\mathbf{R}_{ki} = R_3(\cos \theta_3, \sin \theta_3)$, with $R_{1,2,3} > 0$ and $\theta_{1,2,3} \in [0, 2\pi)$. It is important to point out that ϑ_{ijk} is odd under any odd number of index exchanges. Hence, $\vartheta_{jik} = \vartheta_{kji} = \vartheta_{ikj} = -\vartheta_{ijk}$. At the same time, these exchanges lead to the transformations $\mathbf{R}_{1,2,3} \mapsto -\mathbf{R}_{1,3,2}$, $\mathbf{R}_{1,2,3} \mapsto -\mathbf{R}_{2,1,3}$, and $\mathbf{R}_{1,2,3} \mapsto -\mathbf{R}_{3,2,1}$, respectively. Hence, only antisymmetric terms under these exchanges contribute to ϑ_{ijk} . The definition of ϑ_{ijk} leads to:

$$\begin{aligned} \vartheta_{ijk} &= -4i \int \frac{d\varepsilon}{2\pi} \text{tr} \left[\hat{G}(\varepsilon, \mathbf{R}_{ij}) \hat{G}(\varepsilon, \mathbf{R}_{jk}) \hat{G}(\varepsilon, \mathbf{R}_{ki}) \right] \\ &= -\frac{8(k_F \nu_F)^2}{\sqrt{2\pi}} \frac{\sin[k_F(R_1 + R_2 + R_3) - 3\pi/4]}{\sqrt{k_F^5 R_1 R_2 R_3 (R_1 + R_2 + R_3)^2}} \left(\frac{k_F}{k_0} \right)^6 \left[1 - \left(\frac{k_0}{k_F} \right)^2 \right] \frac{V\Delta^2}{E_F^3} \sin(\theta_1 - \theta_2) \sin(\theta_2 - \theta_3) \sin(\theta_3 - \theta_1). \end{aligned} \quad (40)$$

In the case of an equilateral triangle we can choose $\mathbf{R}_i = a(1, 0)$, $\mathbf{R}_j = a(-1/2, \sqrt{3}/2)$, and $\mathbf{R}_k = a(-1/2, -\sqrt{3}/2)$, which yield $R_{1,2,3} = \sqrt{3}a \equiv R$ and $\theta_1 = -\pi/6$, $\theta_2 = \pi/2$, and $\theta_3 = -5\pi/6$. This gives the following angles $\theta_1 - \theta_2 = \theta_2 - \theta_3 = \theta_3 - \theta_1 = -2\pi/3$.

C. Calculations for Chiral Superconductors

In this section, we repeat the above procedure for a chiral $d + id$ superconductor. Here, $\mu = 0$ and the Fermi level is set by $V = E_F$. We employ the quasi-classical approach also in the upcoming analysis, within which $\Delta \ll E_F$. Therefore, under these conditions, the Hamiltonian of the system takes the approximate form $\hat{H}(k) \approx \xi(k)\tau_3 + \Delta[\cos(2\varphi)\tau_1 + \sin(2\varphi)\tau_2]$, with the linearized normal phase dispersion $\xi(k) = \hbar v_F(k - k_F)$. Note that here $k_F = k_0$, $\hbar v_F = 2E_F/k_F$, while the normal phase density of states at the Fermi level becomes $\nu_F = k_F/2\pi\hbar v_F = k_F^2/4\pi E_F$.

I. Coordinate-Space Matrix Green Function

Once again we employ the definition of the Green function and write:

$$\begin{aligned}\hat{G}(\varepsilon, \mathbf{R}) &\approx -\int_0^\infty \frac{dk k_F}{2\pi} \int_{-\pi}^{+\pi} \frac{d\varphi}{2\pi} e^{ikR \cos(\varphi-\theta)} \frac{i\varepsilon + \Delta \cos(2\varphi)\tau_1 + \Delta \sin(2\varphi)\tau_2 + \xi(k)\tau_3}{\xi(k)^2 + \Delta^2 + \varepsilon^2} \\ &= -\int_0^\infty \frac{dk k_F}{2\pi} \frac{[i\varepsilon + \xi(k)\tau_3] J_0(kR) - \Delta [\cos(2\theta)\tau_1 + \sin(2\theta)\tau_2] J_2(kR)}{\xi(k)^2 + \Delta^2 + \varepsilon^2}.\end{aligned}\quad (41)$$

Also here, we proceed by restricting to the case in which the smallest inter-atom distance exceeds substantially the Fermi wavelength. Under this assumption, the Bessel functions are approximated with their asymptotic form and we find:

$$\begin{aligned}\hat{G}(\varepsilon, R, \theta) &\approx -\sqrt{\frac{2}{\pi k_F R}} \int_0^\infty \frac{dk k_F}{2\pi} \frac{i\varepsilon + \xi(k)\tau_3 + \Delta [\cos(2\theta)\tau_1 + \sin(2\theta)\tau_2]}{\xi(k)^2 + \Delta^2 + \varepsilon^2} \cos\left(kR - \frac{\pi}{4}\right) \\ &\approx -\nu_F \sqrt{\frac{2}{\pi k_F R}} \cos\left(k_F R - \frac{\pi}{4}\right) \int_{-\infty}^{+\infty} d\xi \frac{i\varepsilon + \Delta [\cos(2\theta)\tau_1 + \sin(2\theta)\tau_2]}{\xi^2 + \Delta^2 + \varepsilon^2} e^{\frac{i\xi R}{\hbar v_F}} \\ &\quad -\nu_F \sqrt{\frac{2}{\pi k_F R}} \sin\left(k_F R - \frac{\pi}{4}\right) \int_{-\infty}^{+\infty} d\xi \frac{i\xi\tau_3}{\xi^2 + \Delta^2 + \varepsilon^2} e^{\frac{i\xi R}{\hbar v_F}} \\ &= -\pi\nu_F e^{-\frac{\sqrt{\Delta^2 + \varepsilon^2} R}{\hbar v_F}} \sqrt{\frac{2}{\pi k_F R}} \left\{ \cos\left(k_F R - \frac{\pi}{4}\right) \frac{i\varepsilon + \Delta [\cos(2\theta)\tau_1 + \sin(2\theta)\tau_2]}{\sqrt{\Delta^2 + \varepsilon^2}} - \sin\left(k_F R - \frac{\pi}{4}\right) \tau_3 \right\}.\end{aligned}\quad (42)$$

II. RKKY and Chiral Susceptibilities

We now make use of the above result to find the coefficient of the RKKY term. We remind the reader that, when employing the four component Bogoliubov - de Gennes formalism, one is required to multiply all traces by a factor of 1/2 so to avoid double counting the electronic degrees of freedom. We thus have:

$$\chi(R) = -\int_{-\infty}^{+\infty} \frac{d\varepsilon}{2\pi} \text{tr} \left[\hat{G}(\varepsilon, R, \theta) \hat{G}(\varepsilon, R, \theta + \pi) \right] = \frac{2\nu_F}{\pi R^2} \int_0^\infty d\varepsilon \frac{\varepsilon^2 \sin(2k_F R) - (R/\xi_{sc})^2}{\varepsilon^2 + (R/\xi_{sc})^2} e^{-2\sqrt{\varepsilon^2 + (R/\xi_{sc})^2} R}, \quad (43)$$

where we introduced the superconducting coherence length $\xi_{sc} = \hbar v_F / \Delta$. Here, we are mainly interested in the limit $R \ll \xi_{sc}$. In this case, $|\varepsilon| \gg R/\xi_{sc}$ and we can drop R/ξ_{sc} from the exponential. This approximation yields the result:

$$\chi(R) = \frac{\nu_F}{\pi R^2} \left[\sin(2k_F R) - \frac{\pi R}{\xi_{sc}} \right]. \quad (44)$$

We follow once again the same approach and calculate the chiral susceptibility. We define $\mathbf{R}_{ij} = R_1(\cos \theta_1, \sin \theta_1)$, $\mathbf{R}_{jk} = R_2(\cos \theta_2, \sin \theta_2)$, and $\mathbf{R}_{ki} = R_3(\cos \theta_3, \sin \theta_3)$, with $R_{1,2,3} > 0$ and $\theta_{1,2,3} \in [0, 2\pi)$. After accounting for a factor of 1/2, we pick out the appropriate antisymmetric part and find the expression:

$$\begin{aligned}\vartheta_{ijk} &= -2l \int \frac{d\varepsilon}{2\pi} \text{tr} \left[\hat{G}(\varepsilon, \mathbf{R}_{ij}) \hat{G}(\varepsilon, \mathbf{R}_{jk}) \hat{G}(\varepsilon, \mathbf{R}_{ki}) \right] \\ &= -\frac{2(2\pi)^{3/2} \nu_F^3 \Delta}{\sqrt{k_F^3 R_1 R_2 R_3}} \left\{ \cos\left(k_F R_1 - \frac{\pi}{4}\right) \cos\left(k_F R_2 - \frac{\pi}{4}\right) \sin\left(k_F R_3 - \frac{\pi}{4}\right) \sin[2(\theta_1 - \theta_2)] \right. \\ &\quad + \cos\left(k_F R_2 - \frac{\pi}{4}\right) \cos\left(k_F R_3 - \frac{\pi}{4}\right) \sin\left(k_F R_1 - \frac{\pi}{4}\right) \sin[2(\theta_2 - \theta_3)] \\ &\quad \left. + \cos\left(k_F R_3 - \frac{\pi}{4}\right) \cos\left(k_F R_1 - \frac{\pi}{4}\right) \sin\left(k_F R_2 - \frac{\pi}{4}\right) \sin[2(\theta_3 - \theta_1)] \right\}.\end{aligned}\quad (45)$$